Probabilistic model predicts dynamics of vegetation biomass in a desert ecosystem in NW China

Xin-ping Wang[a,1,2], Benjamin Eli Schaffer[b,1], Zhenlei Yang[c], and Ignacio Rodriguez-Iturbe[b,c,d,e,2]

[a]Shapotou Desert Research and Experiment Station, Northwest Institute of Eco-Environment and Resources, Chinese Academy of Sciences, Lanzhou, Gansu 730000, China; [b]Department of Civil and Environmental Engineering, Princeton University, Princeton, NJ 08544; [c]Department of Biological and Agricultural Engineering, Texas A&M University, College Station, TX 77843-2117; [d]Department of Ocean Engineering, Texas A&M University, College Station, TX 77843-3136; and [e]Department of Civil Engineering, Texas A&M University, College Station, TX 77843-3136

Contributed by Ignacio Rodriguez-Iturbe, May 4, 2017 (sent for review March 7, 2017; reviewed by Paolo D'Odorico and Luca Ridolfi)

The temporal dynamics of vegetation biomass are of key importance for evaluating the sustainability of arid and semiarid ecosystems. In these ecosystems, biomass and soil moisture are coupled stochastic variables externally driven, mainly, by the rainfall dynamics. Based on long-term field observations in northwestern (NW) China, we test a recently developed analytical scheme for the description of the leaf biomass dynamics undergoing seasonal cycles with different rainfall characteristics. The probabilistic characterization of such dynamics agrees remarkably well with the field measurements, providing a tool to forecast the changes to be expected in biomass for arid and semiarid ecosystems under climate change conditions. These changes will depend—for each season—on the forecasted rate of rainy days, mean depth of rain in a rainy day, and duration of the season. For the site in NW China, the current scenario of an increase of 10% in rate of rainy days, 10% in mean rain depth in a rainy day, and no change in the season duration leads to forecasted increases in mean leaf biomass near 25% in both seasons.

ecohydrology | stochastic dynamics | vegetation modeling | climate change impacts | soil moisture

In arid and semiarid ecosystems, successful use of limited water resources is of central importance in determining the evolutionary trends of vegetation. Soil moisture there is the principal limiting factor for vegetation restoration and plays a key role in controlling the spatiotemporal patterns of vegetation regulating the complex dynamics of the climate–soil–vegetation system (1, 2).

Characterizing the vegetation in water-limited ecosystems, with regard to quantity, species composition, and stability, is a long-standing problem in restoration ecology (3). Field surveys and different types of measurements have been taken for decades (4), but they have mostly yielded only descriptive results [e.g., links between soil moisture and accompanying biomass (5)].

Schaffer et al. (3) recently developed an analytical description of the transient joint behavior of plant biomass and soil moisture induced by stochastic rainfall dynamics. These analytical results allow for predictions of ecosystem behavior under changing climate conditions and also illuminate the sensitivities of the dynamics to plant physiology, as well as to climate and soil characteristics that govern the system. The objective of this study is first to test the accuracy of the analytical model under current conditions by comparing its predicted distribution for the biomass density in both the wet and dry seasons with the statistics observed in a long-term field experiment in northwestern (NW) China. Subsequently, using the climate change forecast of the field site, predictions will be made for the seasonal mean biomass and its variability in the future.

Ecosystem Characteristics: Climate, Soil, and Vegetation

Long-term detailed measurements of vegetation dynamics were carried out at the plant level in four plots located at the Shapotou Desert Research and Experiment Station in NW China. Meteorological 60-y records at the station provide an adequate characterization of the rainfall dynamics at the site. The mean annual rainfall is 182.6 mm, of which 82% falls in the rainy season (May 1–September 30) with an observed range between 60 mm and 270 mm and a SD of 57.1 mm. The mean rainfall during the wet season is 149.1 mm and during the dry season is 33.5 mm, with SDs of 51.5 mm and 16.9 mm, respectively.

The arrival of rainfall events is modeled as a Poisson process in which the rate λ_0 (d^{-1}) is constant over the course of a season, but varies between seasons. After accounting for interception (which acts as a censoring process), the rainfall arrival rate is transformed into the infiltration arrival rate λ (2); λ inherits the seasonal characteristics of λ_0, namely constant intraseason and variable interseason values.

The temporal structure within each rainfall event is ignored, with all water modeled as arriving in an instantaneous pulse with random depth. For values of the arrival rate typical of water-limited systems (such as those here), it will be rare for such a process to produce multiple arrivals in a given day, and so the continuous-in-time Poisson process can be correctly understood at the discrete daily scale. In this case, λ_0 (d^{-1}) represents the probability of having rain on a given day, and the distribution of rain depth during a pulse arrival is equivalent to the distribution of rain depth on any rainy day (6); in particular, this distribution is taken to be exponential with mean α (2). The fluctuations of λ_0 and α for both seasons at the site for the period 1956–2015 are shown in Fig. S1.

A detailed description of the field site, its climate, soil, and vegetation is given in *Field Site and Vegetation*. Based on the analysis

Significance

The temporal dynamics of vegetation biomass are of vital importance for evaluating the sustainability of arid and semiarid ecosystems. Field observations indicate that soil moisture and plant biomass fluctuate stochastically with the occurrence of rainfall events. Based on long-term field observations, we find that the dynamics of the vegetation biomass can be quantified by their analytically derived time-dependent probability distribution. This allows for the study of the impact of climate change scenarios on vegetation cover and plant water resource competition. It is found that in a restored desert ecosystem in northwest (NW) China, the growing season leaf biomass is expected to increase by nearly 25% compared to the present.

Author contributions: I.R.-I. designed research; X.-p.W. performed research; X.-p.W., B.E.S., Z.Y., and I.R.-I. analyzed data; X.-p.W., B.E.S., and I.R.-I. wrote the paper; and B.E.S. developed theoretical results.

Reviewers: P.D., University of California, Berkeley; and L.R., Politecnico di Torino.

The authors declare no conflict of interest.

Freely available online through the PNAS open access option.

[1]X.-p.W. and B.E.S. contributed equally to this work.

[2]To whom correspondence may be addressed. Email: irodrigu1@tamu.edu or xpwang@lzb.ac.cn.

This article contains supporting information online at www.pnas.org/lookup/suppl/doi:10.1073/pnas.1703684114/-/DCSupplemental.

Fig. 1. (*Top*) An overview of the site and its vegetation. (*Bottom*) The shrub *A. ordosica*, which is the dominant vegetation type.

of the meteorological data, the mean rainfall arrival rate, λ_0, in the wet season is 0.231 d^{-1}. For the dry season it is 0.073 d^{-1}. The mean daily rainfall depth for a wet day in the wet season is 4.2 mm, and for the dry season it is 2.1 mm (Table S1).

The dominant vegetation is the drought-tolerant shrub *Artemisia ordosica*; photographs of the broader site and this shrub in particular are shown in Fig. 1. Field measurements to estimate the biomass at the end of each season as well as the different plant and soil parameters needed in the analytical computations are described in *Methods*. The values of the climate, soil, and plant parameters are reported in Tables S1 and S2.

The Theoretical Model. The temporal evolution of vegetation biomass per canopy area B may be described by the differential equation

$$\dot{B} = (\alpha\eta - \beta)\, B, \qquad [1]$$

where β is the per-unit biomass loss rate, α is the non–water-limited per-unit assimilation rate, and η is an inhibition function that captures the dependence on water availability for transpiration and assimilation, both modulated by the stomata. In our previous work (3, 7), B has denoted various plant tissue types, but here we are modeling only the leaf component of the vegetation. (Details on the derivation of these dynamics, especially the resolution of and interaction between different tissue types, are given in *Theoretical Model*.) This equation requires a description of the dynamics of water availability for closure, which are provided specifically by a water balance equation for the root zone of the vegetation:

$$A_r\, n\, Z_r \frac{dS}{dt} = -E_m\, \rho\, \eta\, A_c\, B + A_r\, I. \qquad [2]$$

The left-hand side above gives the rate of change of the water volume in the soil. A_r is the root coverage area (i.e., the amount of land surface area with roots beneath it) within the measurement plot, n is the soil porosity, and Z_r is the rooting depth, so that the product $A_r\, n\, Z_r$ is the pore space volume available to store water in the root zone; and S, the relative moisture content, is the fraction actually occupied by water. On the right-hand side, the depth of rain entering the soil per unit time I is multiplied by the root area to give the volumetric input; output (i.e., loss) $E_m\, \rho\, \eta\, A_c\, B$ represents transpiration: The weight of leaf biomass per canopy area B is multiplied by the canopy area of the plot A_c to give the total leaf weight in the plot; this in turn is multiplied by the leaf area per weight constant ρ to give the total plot leaf area; the result is multiplied by the transpiration rate per unit leaf area, given as a maximum rate E_m times the same water limitation factor η that appears in the assimilation rate, which we now write explicitly as a function of soil moisture $\eta(S)$, as in Eq. S28. Rearranging yields

$$\dot{B} = (\alpha\eta(S) - \beta)\, B \qquad [3]$$

$$\dot{S} = -\gamma B \eta(S) + I, \qquad [4]$$

where $\gamma = (A_c/A_r)(E_m\rho/nZ_r)$ and I is given as units of soil storage fraction per time. The values for the derived parameters are given in Table 1. The stochasticity of this infiltration process, with arrival rate λ and a rescaled mean infiltration depth $1/\theta$ (again, expressed as a fraction of the root zone water storage volume), induces a probability density function (pdf) on the biomass–soil moisture state space.

Schaffer et al. (3) showed that for constant rainfall parameters this system allowed for an exact, closed-form steady-state pdf, but also, in recognition of the fact that convergence to this state might take longer than the length of a typical (constant parameter) season, derived an approximation of the system's transient behavior. This approximation exploits the fact that biomass varies on a much slower timescale than soil moisture, so that changes in biomass on an interval of interest (such as a season) involve an integration that tends to average out the soil moisture fluctuations in that interval, allowing for a simple estimation of the marginal pdf of biomass. Formally, this estimate is obtained by setting $\dot{S} = 0$ in the above system, and substituting the soil moisture equation into the biomass equation yields

$$\dot{B} = \frac{\alpha}{\gamma} I - \beta B \qquad [5]$$

so that each unit of infiltrating water is converted immediately to biomass (hence the name given in ref. 3, "no-storage limit")

Table 1. Values of the reduced plant, soil, and climate parameters needed to specify the joint dynamics in Eqs. 3 and 4 and the "no storage" dynamics in Eq. 5 and appearing also in Eqs. 6 and 7

Parameters	Units	Values
α	d^{-1}	0.0196
β	d^{-1}	0.0071
γ	$m^2 \cdot g^{-1} \cdot d^{-1}$	4.44×10^{-5}
s_w	m^0	0.02
s^*	m^0	0.099
λ	d^{-1}	0.182 (wet), 0.045 (dry)
$1/\theta$	m^0	0.022 (wet), 0.011 (dry)
T	d	153 (wet), 212 (dry)

with the conversion ratio—essentially a water use efficiency—of α/γ. This single equation is obtained exactly in the parameter limit where (for given efficiency) the transpiration and assimilation coefficients in the system of Eqs. **3** and **4** are taken to be arbitrarily large, and so it can be considered merely as a simplified, albeit convenient, governing equation for a subset of the parameter space, which is largely how it was discussed in ref. 3. However, this limit has an alternate (and more meaningful) interpretation. The biomass dynamics certainly depend on the availability of water, which may be characterized by the average root zone soil moisture S as in Eq. **3**; this assumes that the transpiration does not depend on the distribution of moisture, so that a single hydrological state variable is sufficient, and the system is closed using the water balance Eq. **4** as discussed. An alternative approach is to note that, for the given (constant) water-to-biomass conversion ratio, each storm represents an injection of potential biomass, and the problem is to determine the amount of it that will be realized and when. The amount is determined by the assumption that, postinterception, all water infiltrating the root zone will be transpired, which is equivalent to saying that transpiration dominates leakage and evaporation within the root zone. The timing of this transpiration is assumed instantaneous, which reflects the fast nature of the soil moisture variations relative to those of the biomass. These two assumptions allow the dynamics to be resolved by a single state variable as in Eq. **5**, without assumptions on the distribution of the root zone soil moisture. Thus, Eq. **5** represents not just a simplification of the two-state-variable model, but also an alternate closure condition. The theory for the underlying dynamics is further elaborated in *Theoretical Model*.

Analysis

Comparison of Field Measurements with Analytical Results. The modeling approach described above is used to examine the biomass response to an alternating regime of wet and dry seasons, as found at the study site. Schaffer et al. (3) showed that for typical dryland parameter values, the end-of-season biomass would be significantly different from that of the constant-parameter steady state (a similar calculation is performed in ref. 8). The system did not have time to adjust to a given season before it ended and the wet–dry cycle started over again. This was also confirmed for the site specifically (Fig. S2). Thus, it is the transient results of ref. 3, corresponding to Eq. **5**, that form the departure point for the analysis here.

The equations describing the pdfs of biomass at any particular time in a wet or dry season and after a given number of consecutive seasonal–annual cycles have taken place are given in Eqs. **S18**–**S21** and plotted in Fig. 2 for the site.

After infinitely many such cycles, the system will have converged to a "seasonal" steady state, where the statistics depend on the point in the year at which measurements are made (i.e., end of wet season, end of dry season), but not on the year in question. Fig. 2 also addresses the question, How long does it take for the seasonal regime to establish itself? This will necessarily depend on the initial state, because a more extreme state will persist for a longer time, but the steady-state distribution provides a useful baseline. To be explicit, suppose the system were exposed to wet (or dry) season conditions for an infinitely long time, allowing it to equilibrate to a sort of upper (or lower) bound on the vegetation state. How many dry–wet cycles will it take to effectively converge from these reference levels? Explicit formulas for the convergence of the moments are given in ref. 3 and in Eqs. **S22**–**S24**, but it is clear graphically from Fig. 2 that the impact of the alternating regime is well established after about 3 y and so beyond this point the seasonal steady state can be said to prevail. The mean and variance of the seasonal steady-state distributions are especially informative and their analytical expressions are given here in Eqs. **6** and **7**. The quantities

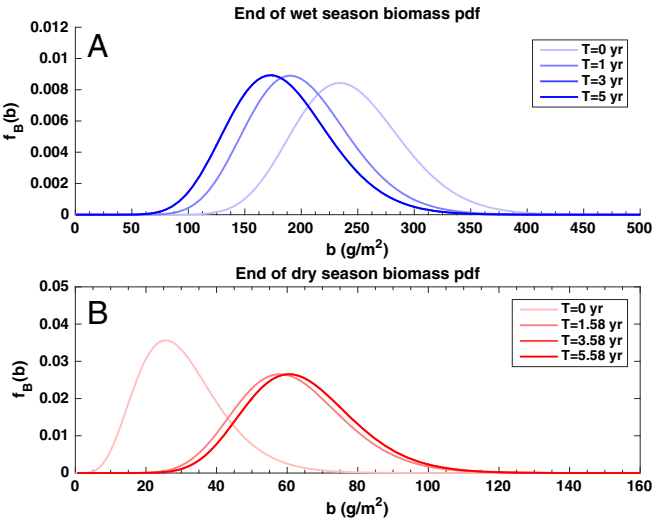

Fig. 2. (*A*) The end of wet season biomass distribution under a regime of alternating wet and dry seasons, starting at wet season steady state, and with each ensuing year consisting of a dry season length of $T_d = 212$ d (0.58 y) followed by a wet season of $T_w = 153$ d (0.42 y). These distributions correspond to global times (in years) $T \in [0, 1, 3, 5]$. (*B*) The effect of the same seasonal regime on the end of the dry season biomass, starting at the dry season steady state, so that the distributions correspond to the global times (in years), $T = 0, 1 + T_d, 3 + T_d, 5 + T_d$.

$p_{(\cdot)} = e^{-\beta_{(\cdot)} T_{(\cdot)}}$, $(\cdot) \in \{d, w, a\}$ can be understood as decay factors, respectively per dry season, per wet season, and per annum, indicating the tendency of each epoch to "wash out" information about the biomass at its start. Note that if (e.g.,) the wet season length were taken to be infinitely long, the end-of-wet season moments would be unaffected by dry season parameters, because any influence initially provided by the dry season would be lost over time:

$$\mu_{\{d,w\}} = \frac{1}{\beta}\left(\frac{\alpha}{\gamma}\right) \times \left(\frac{\lambda_{\{d,w\}}(1-p_{\{d,w\}})/\theta_{\{d,w\}} + \lambda_{\{w,d\}} p_{\{d,w\}}(1-p_{\{w,d\}})/\theta_{\{w,d\}}}{1-p_a}\right) \quad [6]$$

$$\sigma^2_{\{d,w\}} = \frac{1}{\beta}\left(\frac{\alpha}{\gamma}\right)^2 \times \left(\frac{\lambda_{\{d,w\}}(1-p^2_{\{d,w\}})/\theta^2_{\{d,w\}} + \lambda_{\{w,d\}} p^2_{\{d,w\}}(1-p^2_{\{w,d\}})/\theta^2_{\{w,d\}}}{1-p_a^2}\right). \quad [7]$$

Using the parameter values in Table 1, the analytical mean and SD of leaf biomass (leaves, new shoots) per unit of canopy area at the end of dry season and at the end of the wet season are $\mu_d = 64.2$ g·m^{-2}, $\mu_w = 183.1$ g·m^{-2} and $\sigma_d = 15.5$ g·m^{-2},$\sigma_w = 45.6$ g·m^{-2}, respectively. The field measurements of leaf biomass per unit canopy area at the end of wet season are presented in Table S3 for each of the four plots used in this study.

The mean and SD of the biomass at the end of the wet season estimated using all four plots and their different years of measurements are $\mu_w = 185.0$ g·m^{-2} and $\sigma_w = 37.6$ g·m^{-2}, which are both remarkably close to those analytically predicted. (The estimate of the variance is in fact a slight underprediction due to the correlation between measurements made in successive years, although this effect is largely negligible. See *Methods* for details.) The slight overprediction of the variance is to be expected, as

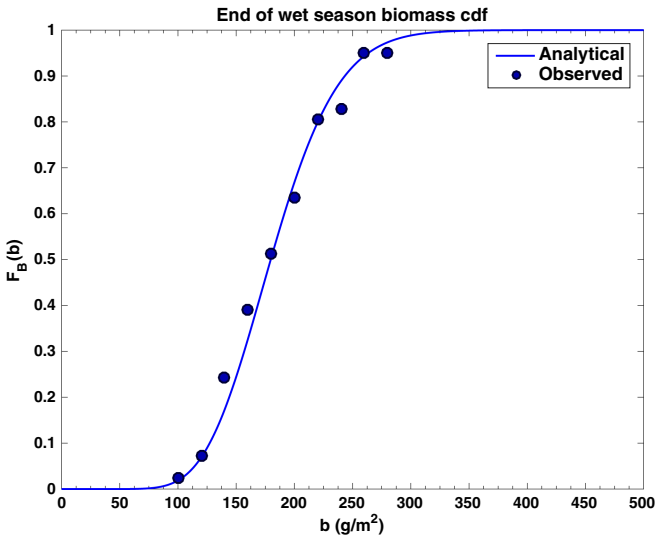

Fig. 3. Comparison of the analytical cumulative distribution of end of wet season biomass (seasonal steady state) with observed data at Shapotou Desert Research and Experiment Station.

the no-storage model removes any temporal buffering effect the soil might have on the rainfall process; a water storage capacity within the plant tissues would also have a buffering, variance-reducing effect not captured by our model. Fig. 3 compares the cumulative distribution function of the leaf biomass data at the end of the wet season with that resulting from the theoretical distribution describing the seasonal steady state at that moment. Again, there is a remarkable agreement between the theory and the data.

There were no previous measurements of biomass at the end of the dry season and thus we performed individual biomass measurements in each of 22 well-established shrubs located in a different 10-m $\times$ 10-m plot at the end of April 2016. The observed results of leaf biomass per unit canopy area at the end of the dry season are shown in Table S4. Because only a single year of dry season data is available, we cannot compute meaningful statistics or form the empirical distribution function. Whereas there is some variability from shrub to shrub, this is not attributable to random hydrological forcing, because each shrub in a small spatial area such as the plot is driven by the same rainfall process. Still, the single-year mean plot biomass may be computed, resulting in $\mu_d = 68.4$ g·m^{-2}, which, perhaps fortuitously, is quite close to the predicted value. Additionally, the interplant variability (which indicates both species-inherent and spatial variability) can be compared with the predicted variability induced by the intermittent rainfall model to determine the relative size of these effects; in *Methods*, we show specifically that interplant contribution to the total variance is small.

The soil moisture was not a major focus of this study, and measurements are not currently available, but because the methodology of ref. 3 provides for it (Eqs. **S26**–**S29**), as a final item we compute the theoretical predictions of the soil moisture distributions that correspond to the end of season biomass states discussed above. These are shown in Fig. 4. Both seasons are characterized by very dry soils (with an overwhelming probability of being at less than 20% saturation), although end of wet season moisture content is higher. This is again indicative of the difference between the seasonal steady state and the "true" steady state, because infinitely long seasons would balance the change in rainfall with a change in transpiring biomass, resulting in the same mean soil moisture for either season.

Impact of Climate Change on Biomass and Soil Moisture Dynamics. The theoretical framework described above allows us to study the impact of climate change on the leaf biomass dynamics arising from changes in the vegetation or climate characteristics. We assume that the type of plants at the site under analysis remains the same and that climate will follow the scenario described in the recent study of Gao et al. (9), which finds a likely increase in the total annual rainfall at the site between 10% and 25%. We also assume that most of the impact on biomass will arise from changes in the rainfall dynamics that in the modeling framework are controlled by the rate of arrival of wet days in each season (λ_0), the mean rainfall depth in a rainy day in each season (a), and the seasons durations (T). The climate scenario to be studied retains the same length of seasons and increases by 10% the λ_0 and the a values for each season. This leads to a total annual rainfall of 219 mm, which is about 21% above the present conditions and in the range found in the climate change study (9). The interception loss is assumed the same ($\Delta = 1$ mm). Many other combinations of changes between λ_0s, as, and Ts could also be studied and this topic is being pursued for a number of regions throughout the world. Fig. 5 shows the seasonal steady-state pdfs for biomass at the end of the wet and dry seasons under the conditions of the new climate scenario. They should be compared with those in Fig. 2 describing the present conditions. The mean values and SDs are now $\mu_w = 226.6$ g·m^{-2}, $\mu_d = 80.1$ g·m^{-2} and $\sigma_w = 53.2$ g·m^{-2}, $\sigma_d = 18.2$ g·m^{-2}. The steady-state pdfs for soil moisture under the conditions of the above climate change scenario experience very little change with respect to the present ones shown in Fig. 4; the additional rainfall predicted under climate change is largely offset—from the point of view of the soil water balance—by the larger amount of transpiring vegetation. Thus, the first-order effects of climate change would be on the vegetation, with the soil moisture experiencing second-order effects.

Finally, we point out that these predictions ostensibly address the biomass and soil moisture properties that would occur if the climate change scenario prevailed in place of the current one. We have not explicitly discussed the (temporally structured) transition from one regime to another, but in practice this distinction is of little consequence. The characteristic biomass adjustment timescale is on the order of $1/\beta$ (with full adjustment

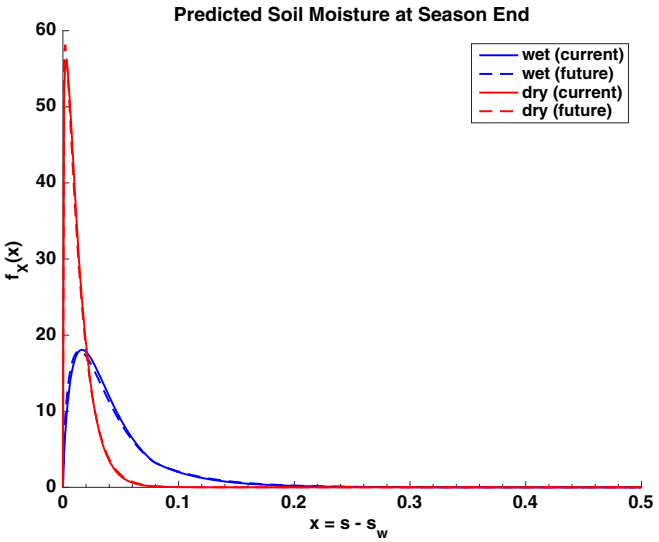

Fig. 4. Seasonal steady-state pdf of relative soil moisture ($x = s - s_w$) for wet and dry season conditions, under both the current and climate change rainfall scenarios.

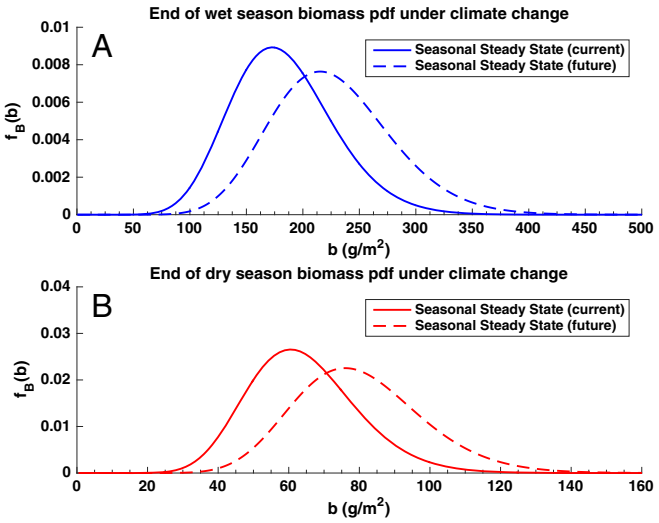

Fig. 5. (*A* and *B*) Similar to Fig. 2 for a climate change scenario where arrival rate of wet days and the mean rainfall depth in a rainy day have increased 10% each in both seasons. These conditions yield an increase in annual rainfall of 21%, which is in the range forecasted by the study of Gao et al. (9).

even from a relatively extreme state occurring in <3 y, as in Fig. 2), whereas the climate is predicted to change on the decadal scale, so the biomass at future times will tend to stay well adjusted to the climate at those times; e.g., Eqs. **6** and **7** for the mean and variance in a given year would be well determined by using the parameters prevailing in that year, the longer history being "forgotten" by the biomass process before the climate could change very much. However, we may add the caveat that the biomass considered here is the leaf biomass; the dynamics of seed germination/new plant emergence and wood growth might occur on timescales comparable to the climate change timescale.

Discussion

The analytically derived mean and SD of leaf biomass at the end of the wet season matches very closely with those measured in the field. Our single year of dry season data are also consistent with the data, although by itself it does not permit a good estimate of the distribution. Moreover, the analytical cumulative distribution of leaf biomass at the end of the wet season also agrees very well with the long-term data. This close agreement gives confidence to the values predicted under the climate change scenario studied for the site. In the wetter conditions considered in the scenario the mean biomass at the end of the wet season is 24% larger than the present one. For the dry season the change in mean biomass is 25%. The predicted increase in leaf biomass is thus very significant and carries important consequences for the structure of the ecosystem and for the future reforestation of other sites in the region. The predicted increase in the SD of leaf biomass is about 17% for each season and thus the coefficient of variation is reduced by near 6% for each season.

The above predictions are assuming that the increase in total rainfall results from an increase of 10% in both λ_0 and a for both seasons and that the duration of the seasons as well as the plant characteristics remain the same. Other scenarios can also be studied. If one wished to study a scenario where λ_0 and a remain the same and the 21% forecasted increase in annual rainfall results from an increase of 30.4% in the duration of the wet season, the predicted biomass at the end of the wet or dry season would be 205.0 g·m^{-2} and 84.3 g·m^{-2}, respectively, which is quite different from that under the scenario considered here. This illustrates the importance of understanding the statistical structure of the rainfall and not just its mean values. We emphasize that this structure affects not only the shape of the biomass distribution (i.e., its higher-order moments), but also the mean biomass value; the nonlinear, threshold-type nature of the interception results in a greater fraction of water reaching the root zone when the mean rainfall depth increases, so that the mean biomass increases superlinearly (hence the 24% predicted increase with a 21% increase in annual rainfall, as discussed in the previous section).

Methods

Field Observations of the Desert Shrub Ecosystem. Four experimental plots of 10×10 m^2—identified by the year when revegetation was initiated—were studied in regard to their changes in plant biomass throughout the years. The shrub canopy projection area was calculated by taking the longest and shortest diameters through the center of the fullest part of the canopy. The biomass per unit canopy projection area at the end of wet season is calculated from a site-specific previously established empirical relationship between leaf biomass and canopy projection area (10, 11). This characterization was carried out at the individual plant level for the four plots in the years between 1981 and 1998. The percentage of the canopy coverage over the total area of the plot is the sum of the canopy areas divided by the plot area. No similar data were available for biomass at the end of the dry season. Thus, a preliminary estimation was carried out in this case for 2016. The biomass at the end of the dry season of the year 2016 was estimated by direct harvesting of one plot (10×10 m^2) outside the long-term vegetation-monitoring plots because such a harvesting method is prohibited in those plots. With the measured leaf biomass and from the canopy projection area we calculate the leaf biomass per unit area of canopy coverage (10, 11). The measured biomass per unit canopy area and the canopy coverage area at the end of the wet season for the period 1981–1998 are given in Table S3 for all four plots. The corresponding values at the individual shrub level corresponding to the end of the dry season in 2016 are given in Table S4.

The active root zone depth (Z_r) where over 90% of the roots are contained was measured by ditches to a depth of 2 m with a width of 0.5 m across the center area where the shrub grows. During this process observations were made of the root distribution. Saturated soil conductivity (K_s) was obtained via in situ infiltration measurements through a tension disk infiltrometer (12).

Canopy interception loss ($\Delta = 1$ mm) was estimated as the difference between open-field rainfall and throughfall (13).

The transpiration rate (E) and photosynthesis rate (P_n) were measured on clear sunny days from the sunrise time at around 6 AM (local time) to the sunset time around 7 PM at time intervals of 1 h. Each measurement was taken on three mature shrubs. For each shrub, three labeled leaves from the top, middle, and low canopy positions were selected under non–water-limited conditions. Using a portable Li-6400 gas analysis system, the uptake of CO_2 of each labeled leaf was estimated (Li-Cor Inc.) and leaf area of the labeled leaves was obtained using the Li-3000 area meter after the gas exchange experiment was concluded. Thus, the P_n and E per unit leaf area were then calculated. The maximum P_n and E needed for the analytical calculations were then determined from the hourly variations of P_n and E from 6 AM to 7 PM. P_n is the rate of the uptake of CO_2 per unit leaf area, and thus the net assimilation (A_m) per unit leaf area is calculated by subtracting the weight of carbon from the total molecular weight of CO_2 on the basis of the maximum P_n. The maximum daily transpiration, E_m and maximum daily net assimilation, A_m are then scaled to the daily duration of transpiration and photosynthesis activities, which is estimated in 13 h for the study area.

The root respiration coefficient, R_r, the fraction of daily assimilation lost in respiration by roots per unit mass of roots, was calculated from root respiration rates (obtained using the portable Li-6400 gas analysis system) and dry root weights. The other plant traits, e.g., the specific leaf area (ρ), leaf mass ratio (f_L), growth yield (Y_g), and senescence rate (q), were determined during the field survey (14). More details about the procedures are given in *Field Observations*. The values of the parameters are shown in Table S2.

Correcting the Variance. We have mentioned in passing two corrections to the variance that might arise, due to the variability between individual plants (i.e., a spatial correction), as well as to the interannual correlations

of the measurements (i.e., a temporal correction). We address both types here and show that they are small.

We begin with the interplant variability. The most likely source of such variability in our model is that each plant may have a different value of the term α/γ, reflecting either variability in the efficiency of the plant (the amount of biomass realized per unit of water) or, more likely, variability in the horizontal spread of the root zone, which translates into a variability in the amount of water provided to the plant by each rainfall event. As shown in Eqs. S35 and S36, variability in this quantity scales the biomass of the corresponding plant by a fixed amount, but otherwise does not change its probabilistic behavior in time. If we let $B_0(t)$ denote the biomass corresponding to the values α/γ used previously, we can write for plant i

$$B_i(t) = Z_i B_0(t), \quad [8]$$

where Z_i is the relative efficiency, now permitted to have a spread around the reference value (i.e., the mean value) of unity. Each measurement of biomass at a given point of time involves an averaging over n_p plants,

$$B(t) = \frac{1}{n_p}\sum_{i=1}^{n_p} B_i(t) = \hat{\mu}_Z\, B_0(t), \quad [9]$$

seen above to separate as a product of the average relative efficiency with the reference biomass (which is, to reiterate, the one corresponding to the efficiency value used throughout this paper). The total variance is obtained by conditioning on the value of the random variable $\hat{\mu}_Z$, using the law of total variance (see Eqs. S35–S40 for details):

$$\mathrm{Var}[B] = \sigma_B^2 + \mathrm{Var}[\hat{\mu}_Z]\,\mu_B = \sigma_B^2\left(1 + \mu_B^2\,\frac{1}{n_p}\,\frac{\sigma_Z^2}{\sigma_B^2}\right). \quad [10]$$

Here, σ_B^2 is the analytical variance induced by the stochastic rainfall process. The second term in the parentheses is the fractional variance correction due the interplant variability, which depends on two new quantities: the variance of the relative efficiency σ_Z^2, determined by the detailed, plant-by-plant measurements made in the dry season of 2016 as $\sigma_Z^2 \approx 0.056$, and also the number of plants n_p used to determine each year's biomass. The plot in which the 2016 dry season measurements were made had 22 plants, and the other plots had a comparable number, so that the variance correction from this source is about 1%.

We turn now to the temporal correction; because of the interannual correlations of the measurements, the standard estimate of the variance will be biased. In particular, because the correlations are positive, it will on average yield an underestimate. The standard estimator of the variance for n independent measurements X_i is

$$\hat{\sigma}^2 = \frac{1}{n-1}\sum_{i=1}^{n}(X_i - \hat{\mu})^2. \quad [11]$$

Taking the expectation of both sides gives

$$\mathbb{E}[\hat{\sigma}^2] = \sigma^2 - \frac{1}{n(n-1)}\sum_{i=1}^{n}\sum_{j\neq i}\sigma_{i,j}^2. \quad [12]$$

As shown in Eq. S33, the autocovariance between measurements i, j is $p_a^{|i-j|}$, where as before p_a is a decay factor (Eqs. 6 and 7). Substituting and summing the resultant geometric series gives the result in Eq. 13, whence we see that the error is about 1% (with $n = 14$, using all data shown in Table S3):

$$\mathbb{E}[\hat{\sigma}^2] \approx \sigma^2\left(1 - \frac{2p_a}{n}\right). \quad [13]$$

Determining the Rainfall Parameters. As a final point, we address the question of how to accurately determine the rainfall parameters. The values used thus far were obtained by averaging over a relatively long time period, 1956–2015, whereas our biomass measurements were made over the shorter period 1981–1998, with the bulk of the measurements in 1989–1998 when all four plots were incorporated. To justify this, let us consider what would happen if we tried to determine the rainfall parameters from a more targeted time interval, e.g., the 10 y of 1989–1998. To be concrete, let us consider the determination of the wet season rainfall arrival rate $\lambda_{0,w}$. Suppose the true value were as estimated above, $\lambda_{0,w} = 0.231\ \mathrm{d}^{-1}$; then we can compute the sampling error as follows. The variance over time T of the number of rainfall arrivals for such a Poisson process is

$$\sigma_N^2 = \lambda_{0,w}\,T \quad [14]$$

and the variance in the corresponding estimate $\hat{\lambda}_{0,w} = N(T)/T$ is

$$\sigma_{\hat{\lambda}_{0,w}}^2 = \frac{\lambda_{0,w}\,T}{T^2} = \frac{\lambda_{0,w}}{T}. \quad [15]$$

If we made this estimate over 10 y of wet seasons, then $T = 10\,T_w$, and we would find that $\sigma_{\hat{\lambda}_{0,w}} = 0.0123\ \mathrm{d}^{-1}$, and so the size of the 2σ range would be 21% of the true value, which is rather large. Thus, in using the full rainfall history to estimate the parameters, we have made a tradeoff: We reduce this statistical imprecision of the determination, but we necessarily risk averaging out genuine variations. A more detailed climatological history is beyond the scope of this work, although any reader concerned by this method may be assuaged by the fact if we did restrict our estimation window to, e.g., 1989–1998, we would get (for the {wet, dry} season, respectively) $a = \{4.33, 2.41\}$ mm, $\lambda_0 = \{0.221, 0.0778\}\ \mathrm{d}^{-1}$, $\lambda = \{0.175, 0.0514\}\ \mathrm{d}^{-1}$, yielding the biomass prediction $\mu_B = \{184.5, 71.6\}\ \mathrm{g{\cdot}m^{-2}}$, $\sigma_B = \{46.2, 17.6\}\ \mathrm{g{\cdot}m^{-2}}$; these values are almost identical to the stated results.

ACKNOWLEDGMENTS. The authors are grateful to colleagues at Shapotou Desert Research and Experiment Station, Chinese Academy of Sciences for their help in the long-term field observation data. This work was funded by the National Natural Science Foundation of China (Grants 41530750 and 41371101), the National Science Foundation (Grant 1514606, "Mathematical Methods for Water Problems"), and the Texas Experimental Engineering Station of Texas A&M University.

1. Porporato A, D'odorico P, Laio F, Ridolfi L, Rodriguez-Iturbe I (2002) Ecohydrology of water-controlled ecosystems. *Adv Water Resour* 25:1335–1348.
2. Rodriguez-Iturbe I, Porporato A, Ridolfi L, Cox DR, Isham V (1999) Probabilistic modeling of water balance at a point: The role of climate, soil, and vegetation. *Proc R Soc Lond* 455:3789–3805.
3. Schaffer BE, Nordbotten JM, Rodriguez-Iturbe I (2015) Plant biomass and soil moisture dynamics: Analytical results. *Proc R Soc A* 471:20150179.
4. Li XR, Xiao HL, Zhang JG, Wang XP (2004) Long-term ecosystem effects of sand-binding vegetation in the Tengger desert, Northern China. *Restor Ecol* 12:376–390.
5. Li X, Kong D, Tan H, Wang X (2007) Changes in soil and vegetation following stabilisation of dunes in the southeastern fringe of the Tengger desert, China. *Plant Soil* 300:221–231.
6. Rodriguez-Iturbe I, Porporato A (2004) *Ecohydrology of Water-Controlled Ecosystems* (Cambridge Univ Press, Cambridge, UK).
7. Zea-Cabrera E, Iwasa Y, Levin S, Rodríguez-Iturbe I (2006) Tragedy of the commons in plant water use. *Water Resour Res* 42:W04D02.
8. Nordbotten JM, Rodriguez-Iturbe I, Celia MA (2007) Stochastic coupling of rainfall and biomass dynamics. *Water Resour Res* 43:W01408.
9. Gao X, Shi Y, Zhang D, Giorgi F (2012) Climate change in China in the 21st century as simulated by a high resolution regional climate model. *Chin Sci Bull* 57:1188–1195.
10. Wang Q (1994) Quantitative models of estimating biomass of Artemisia ordosica and Caragana intermedia. *Grassl China* 1:49–51.
11. Wang Q, Li B (1994) Preliminary study on biomass of Artemisia ordosica community in Ordos Plateau sandland of China. *Acta Phytoecological Sinica* 18:347–353.
12. Wang XP, et al. (2013) Comparison of hydraulic behaviour of unvegetated and vegetation-stabilized sand dunes in arid desert ecosystems. *Ecohydrology* 6:264–274.
13. Wang XP, Li XR, Zhang JG, Zhang ZS, Berndtsson R (2005) Mesure de l'interception de la pluie par des arbustes xérophiles sur des dunes de sable replantées [Measurement of rainfall interception by xerophytic shrubs in re-vegetated sand dunes]. *Hydrolog Sci J* 50:897–910.
14. Zhou H, Wang Y, Fan F, Fan H (2013) Eco-physiological responses and related adjustment mechanisms of Artemisia ordosica and Caragana korshinskii under different configuration modes to precipitation variation. *Chin J Appl Ecol* 24:32–40.
15. Berndtsson R, et al. (1996) Soil water and temperature patterns in an arid desert dune sand. *J Hydrol* 185:221–240.
16. Ling Y, Qu J, Hu M (1993) Crust formation on sand surface and microenvironmental change [j]. *Chin J Appl Ecol* 4:393–398.
17. Li X, Zhang Z, Huang L, Wang X (2013) Review of the ecohydrological processes and feedback mechanisms controlling sand-binding vegetation systems in sandy desert regions of China. *Chin Sci Bull* 58:1483–1496.
18. Zhang L, Wang X, Liu L, Huang Z, Liu X (1997) Study on gas exchange characteristics of main constructive plants A. ordosica and C. korshinskii in Shaptou region. *Acta Ecologica Sinica* 18:133–137.
19. Kobayashi T, Liao RT, Li SQ (1995) Ecophysiological behavior of Artemisia ordosica on the process of sand dune fixation. *Ecol Res* 10:339–349.
20. Návar J, Nájera J, Jurado E (2002) Biomass estimation equations in the tamaulipan thornscrub of north-eastern Mexico. *J Arid Environ* 52:167–179.

21. Návar J, Méndez E, Dale V (2002) Estimating stand biomass in the tamaulipan thornscrub of northeastern Mexico. *Ann Forest Sci* 59:813–821.
22. Northup B, Zitzer S, Archer S, McMurtry C, Boutton T (2005) Above-ground biomass and carbon and nitrogen content of woody species in a subtropical thornscrub parkland. *J Arid Environ* 62:23–43.
23. Li SL, Zuidema PA, Yu FH, Werger MJ, Dong M (2010) Effects of denudation and burial on growth and reproduction of Artemisia ordosica in Mu Us sandland. *Ecol Res* 25:655–661.
24. Norman J, Garcia R, Verma S (1992) Soil surface CO_2 fluxes and the carbon budget of a grassland. *J Geophys Res Atmos* 97:18845–18853.
25. Kucera C, Kirkham DR (1971) Soil respiration studies in tallgrass prairie in Missouri. *Ecology* 52:912–915.
26. Gifford RM (2003) Plant respiration in productivity models: Conceptualisation, representation and issues for global terrestrial carbon-cycle research. *Funct Plant Biol* 30:171–186.
27. Zhang ZS, et al. (2008) Distribution and seasonal dynamics of roots in a revegetated stand of Artemisia ordosica kracsh. in the Tengger desert (North China). *Arid Land Res Manag* 22:195–211.
28. Qin Y, et al. (2008) Fine root biomass seasonal dynamics and spatial changes of Sabina vulgaris and Artemisia ordosica communities in Mu Us sandland. *J Desert Res* 28:455–461.